Received: 23 February 2023 | Revised: 8 April 2023 | Accepted: 9 April 2023

DOI: 10.1111/jace.19172

Journal of the American Ceramic Society

RESEARCH ARTICLE

The peak-shift method for the description of structural relaxation in glassy materials: a critical review

Roman Svoboda

Department of Physical Chemistry, University of Pardubice, Pardubice, Czech Republic

Correspondence
Roman Svoboda, Department of Physical Chemistry, University of Pardubice, Studentska 573, 532 10 Pardubice, Czech Republic.
Email: roman.svoboda@upce.cz

Funding information
Ministry of Education, Youth and Sports of the Czech Republic, Grant/Award Number: LM2023037

Abstract

Nowadays, the glass transition kinetics is most commonly described in terms of the Tool–Narayanaswamy–Moynihan (TNM) model. Evaluation of one of the most prominent features of the structural relaxation motions—the relaxation nonlinearity—was traditionally done using the peak-shift (PS) method. This paper introduces, for the first time, extensive testing of the PS method by means of theoretical simulations for all practically observable types of structural relaxation behavior and all types of glassy/amorphous materials (tested range of the glass transition temperatures: −55 to 1000°C; tested range of the relaxation activation energies: 300–1300 kJ·mol^{-1}). For the majority of types of structural relaxation behavior, the PS method tends to slightly overestimate the value of the TNM nonlinearity parameter x (by ∼ 0.05–0.10). In the specific cases of the highly linear behavior (↑ x) combined with a broad distribution of relaxation times, the PS method systematically vastly underestimates the value of x. A new, improved temperature program was proposed for the PS method, eliminating the major intrinsic drawback of the originally proposed version of the PS methodology. In addition, based on the comparison between the theoretically simulated and real-life experimental data, a new approach (based on the characteristic PS dependence shape) was introduced to estimate the width of the relaxation times distribution.

KEYWORDS
aging, glass transition, kinetics, theory, thermal analysis

1 | INTRODUCTION

Structural relaxation is one of the critical processes associated with every non-crystalline material.[1–13] Knowledge of its kinetics allows predicting the temperature dependence of the occurrence of the glass transition phenomenon—the transformation between the liquid-like undercooled liquid state and solid-like frozen-in the glassy state. Furthermore, the structural relaxation kinetics also determines the rate of the structural re-ordering under different circumstances, which is crucial for assessing the long-term stability of the non-crystalline materials. Note that the process of structural relaxation affects not only the volume of the sample but also many of its mechanical and optical properties.[11–21] The structural relaxation data are nowadays usually described in terms of the Tool's concept of fictive temperature T_f,[22] which represents the structural state of the material, and is defined as the temperature of the undercooled liquid with the same structure as is that of the relaxing glass. This concept was very conveniently

utilized in the phenomenological Tool–Narayanaswamy–Moynihan (TNM) relaxation model[22–24]:

$$\frac{T_f(t)-T_f(\infty)}{T_f(0)-T_f(\infty)}=\exp\left[-\left(\int_0^t\frac{dt}{\tau}\right)^{\beta}\right] \quad (1)$$

$$\tau\left(T,T_f\right)=A_{\mathrm{TNM}}\cdot\exp\left[x\frac{\Delta h^*}{R_gT}+(1-x)\frac{\Delta h^*}{R_gT_f}\right], \quad (2)$$

where the indices "0" and "∞" correspond to the initial and final/equilibrium states, respectively, t is time, T is temperature, τ is relaxation time, R_g is the universal gas constant, Δh^* is the apparent activation energy, A_{TNM} is the pre-exponential constant, $x\,(0<x\leq 1)$ is the nonlinearity parameter, and $\beta\,(0<\beta\leq 1)$ is the non-exponentiality parameter. The fictive temperature T_f from Equation (1) is, in practice, replaced by various physical quantities, with the two most commonly used being the volume (dilatometric measurements) and enthalpy (calorimetric measurements).

Enumeration of Equations (1) and (2) can be narrowed to determine the four key TNM parameters—Δh^*, A, β, and x. Whereas a simultaneous determination of all four TNM parameters can be done through curve-fitting,[25] this approach has several serious drawbacks. First, the parameters are relatively highly correlated, and multiple sets of different TNM parameters combinations can be found equally appropriate in the case of inadequately chosen experimental data that are being fit (this is especially true for the single-curve optimizations). Second, the curve-fitting procedure is susceptible to even minor distortions of the experimental data that can arise either as the consequence of the unideal measurement conditions (thermal lags) or can be intrinsic to the measurement system (instrumental artifacts and artificial corrections introduced by the companies manufacturing the instruments). For this reason, a number of alternative methods (usually based on integration or linearization approaches) have been developed in order to independently determine individual TNM parameters. The majority of these methods have been recently revisited, thoroughly tested, and modernized: for example, the determination of Δh^* from the so-called constant ratio (CR) cyclic experiments[26] has been developed and adjusted for the evaluation of the temperature corresponding to the maximum of the relaxation peak T_p (see Figure 1A), which led to a derivation of very accurate, precise, and robust methodology.[27] The Moynihan approach[6] to the determination of Δh^* has been tested and critically reviewed in,[28] introducing the conditions for accurate and undistorted measurements. Another famous method, the simulation-comparative approach to the determination of the non-exponentiality parameter β, has been improved and extended in,[29,30] resulting in a novel methodology, that is, significantly more robust and precise and can be used for a simultaneous determination of the x and β TNM parameters.

Considering the most famous methods derived for determining the TNM parameters, this leaves only the peak-shift (PS) method (derived in 1984 by Hutchinson[31,32] as a tool for the determination of the TNM nonlinearity parameter x) in its original unmodified form, being practically untouched for many decades. In this paper, we aim to thoroughly test the PS method by means of theoretical simulations in order to determine the potential limitations of its applicability.

2 | THEORY OF THE PS METHOD

The PS method utilizes the derivative data (in the $dT_f{\cdot}dT^{-1}$ form—similar to those depicted in Figure 1A) corresponding to the four-step temperature cycles. During these cycles, the sample is first shortly annealed at the initial temperature T_{ini} (well above the glass transition temperature T_g, for the sample to be in equilibrium) to fully erase the previous thermal history and achieve thermo-structural equilibrium. In the second step, the sample is quickly cooled at rate q^- from T_{ini} to the annealing temperature T_a, which is below T_g. In the third step, the sample is annealed at T_a for a certain time t_a. In the fourth step, the sample is heated back to T_{ini} at a heating rate of q^+. The temperature T_a needs to be selected for the relaxation to proceed reasonably quickly; this will be further discussed in Section 3. The main variable within the series of the four-step cyclic experiments is the annealing time t_a—see Figure 1B for the schematic overview of the four-step cyclic temperature program; the $dT_f{\cdot}dT^{-1}$ signal corresponding to the heating scans is then shown in Figure 1C. Regarding the evaluated quantities, for each relaxation peak the temperature corresponding to the maximum of the relaxation peak T_p and the excess enthalpy δ_{H} are determined. The excess enthalpy is determined as follows:

$$\delta_H=\Delta H-\Delta H_0 \quad (3)$$

where ΔH_0 is the minimum enthalpy achieved during the cycle with $t_a=0$, and ΔH stands in this equation for the excess enthalpy achieved during the cycle when relaxation proceeded under the defined conditions (T_a, and $t_a\neq 0$). A graphical representation of the δ_{H} determination is shown in Figure 1D.

The basis of the PS method was originally derived in terms of the Kovacs–Aklonis–Hutchinson–Ramos (KAHR) phenomenological structural relaxation model.[3] However, parametrically, the KAHR model is very similar

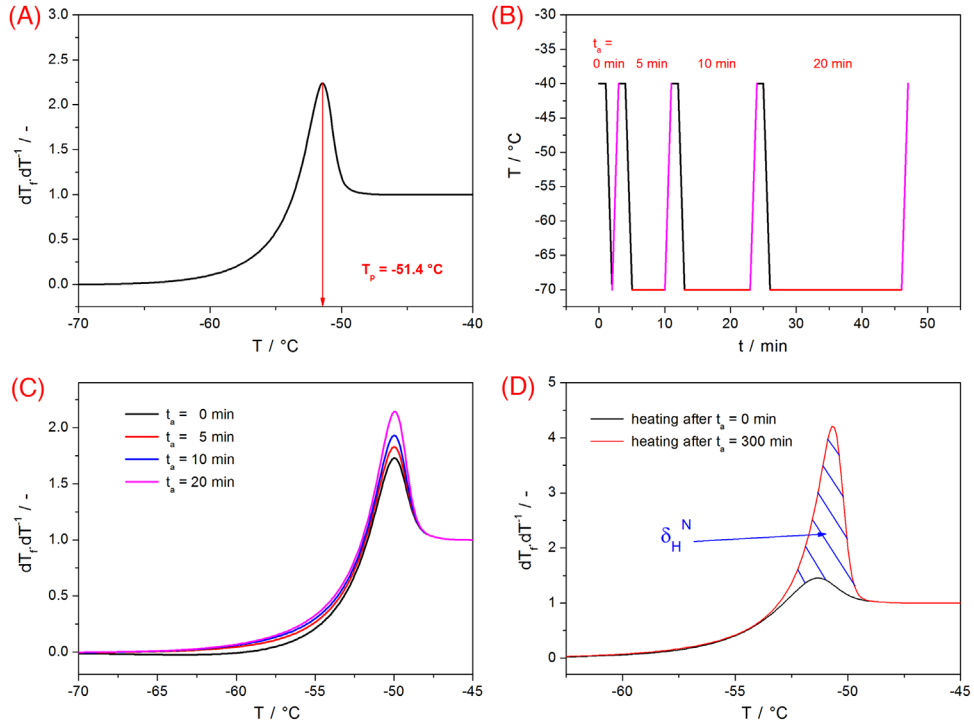

FIGURE 1 (A) Depiction of the typical simulated relaxation peak and of the corresponding evaluation of T_p. (B) Example of the PS temperature program (first four cycles)—red lines represent annealing steps (characterized by T_a and t_a) and the magenta steps represent the heating scans that are used for the evaluation of T_p and $\delta_H{}^N$. (C) Example heating scans curves corresponding to the temperature program displayed in graph C. (D) Schematic representation of the $\delta_H{}^N$ evaluation. PS, peak-shift.

to the TNM model: the KAHR model utilizes the concept of deviations from the equilibrium state (similar to the Tool's T_f concept), the KAHR model employs summation over each individual deviation corresponding to the given element of glassy matrix (analogy of the TNM non-exponentiality parameter β), the KAHR model utilizes the nonlinearity parameter x, and the KAHR model also includes the apparent activation energy in the following form:

$$\theta \approx \frac{\Delta h^*}{RT_g^2}. \tag{4}$$

The PS method defines the following reduced (normalized) variables: Q^-, D_H, and Q^+, where $Q^- = \theta \cdot q^-$, $D_H = \theta \cdot \delta_H / \Delta C_p$, and $Q^+ = \theta \cdot q^+$. The dependence of T_p on these variables can then be expressed by the partial derivatives:

$$s(Q^-) = \theta \left(\frac{\partial T_P}{\partial \ln |q^-|} \right)_{\delta_H, q^+}, \tag{5}$$

$$s(D_H) = \Delta C_p \left(\frac{\partial T_P}{\partial \delta_H} \right)_{q^-, q^+}, \tag{6}$$

$$s(Q^+) = \theta \left(\frac{\partial T_P}{\partial \ln |q^+|} \right)_{\delta_H, q^-}. \tag{7}$$

It was further shown[33] that a master curve/function can be constructed in the following fashion:

$$F(x) = s(D_H) = s(Q^+) - 1 = -s(Q^-), \tag{8}$$

where its interrelation with the nonlinearity parameter is as follows:

$$F(x) = x^{-1} - 1. \tag{9}$$

In practice, the combination of Equations (6) and (9) is used for the determination of x. It is, however important to mention that, according to,[31,32] this expression holds only for the conditions of a well-stabilized glass. For the annealed glass, the relaxation peaks were in[31,32] denoted as "main peaks", whereas the shorter annealings led to the occurrence of the so-called "upper peaks". Unfortunately, the only way of distinguishing between these two types of relaxation peaks was based on the behavior (linearity and non-zero slope) of the $s(D_H)$ dependence. The cyclical experiments have to be therefore iteratively prolonged and repeated until the required behavior/dependence is obtained—this aspect of the experimental setup will be further discussed in Section 4.1.

3 | RESULTS

Several examples of literature reports on the utilization of the PS method can be found in.[34–40] However, these examples are not numerous, and the results are often not confirmed by an alternative method but rather used as an absolute basis for the determination of other TNM parameters. Most importantly, the materials experimentally investigated by means of the PS method represent only a very limited sample of the possible types of structural relaxation behavior. In order to explore the performance of the PS method for a large variety of experimental conditions as well as for all archetypal relaxation patterns, theoretical calculations were employed to simulate a large number of four-step cyclic data. The theoretical simulations were based on the TNM model, with the numerical algorithm in the form of Equation (10) for the non-isothermal segments and Equation (11) for the isothermal segments:

$$T_{f,n} = T_0 + \sum_{j=1}^{n} \Delta T_j \left\{ 1 - \exp\left[-\left(\sum_{k=j}^{n} \Delta T_k / q_k \tau_k \right)^{\beta} \right] \right\}. \tag{10}$$

$$T_{f,n} = T_0 + \sum_{j=1}^{n_A} \Delta T_j \left\{ 1 - \exp\left[-\left(\sum_{k=n_A}^{n} \Delta t_{e,k} / \tau_k \right)^{\beta} \right] \right\}, \tag{11}$$

where T_0 is the initial equilibrium temperature, and t_e is the annealing time. The fundamental basis of the algorithm is in detail explained in.[25] The $\Delta T = 0.1$ K (precision 10 times better than suggested in[25]) was used for the present simulations.

The first batch of testing was performed for a low-T_g material behavior (typical for, e.g., polymers[41]) as one extreme of the structural relaxation archetypes—with $\Delta h^*/R = 40$ kK, $\ln(A/s) = -180$ and $T_g \approx -55$°C. Note that the results obtained in these tests will be generalized in Section 4 to derive universal conclusions regarding the performance of the PS method for all relevant glassy materials. The annealing temperature was set to $T_a = -70$°C, that is, ca. 15°C below T_g; the annealing times $t_a = 0$, 10, 100, 300, 10^3, 10^4, 10^5, $3{\cdot}10^5$, and 10^6 were set to cover the whole range of practically/experimentally applicable times (+ the last one that rather corresponds to some left-over samples from previous study picked up after long-term storage). These sets of PS cycles (each cycle corresponding to the four-step experiment with given t_a as listed above → the whole set containing nine cycles) were simulated for all combinations of relevant x and β values (both varying in the 0.3–0.9 range with the step of 0.1) to cover all types of structural relaxation behavior. This resulted in 49 sets and 441 PS cycles in total. Note that materials with the x and β values < 0.3 are quite rare, the overall structural relaxation kinetics cannot be really evaluated reliably (for very low β), or (for very low x) the features of the PS method are exactly the same as presented for the cases with $x = 0.3$.

Two examples of the simulated and evaluated PS method data are shown in Figure 2—whereas the data for the $\beta = 0.7$ and $x = 0.4$ (left column) represent quite typical material with the rather narrow distribution of relaxation times (high β) and rather high dependence of relaxation movements on the surrounding structure (low x), the second depicted combination of $\beta = 0.5$ and $x = 0.5$ (left column) shows a more exotic example with $\beta \approx x$. The first set of graphs (Figure 2A,B) shows the temperature evolution of T_f (integral data) during the heating scans (last steps of the four-step PS cycles) following the isotherms with different t_as. Note the similar scaling of the two graphs, which shows that the increase of β and simultaneous decrease of x lead to a significantly more pronounced shift of T_p to higher temperatures with increasing t_a. The second set of graphs (Figure 2C,D) show the corresponding derivative data, that is, the temperature dependence of $dT_f{\cdot}dT^{-1}$. Both graphs are zoomed-in on the low $dT_f{\cdot}dT^{-1}$ values to distinguish between the most interesting differences. The full-scale graphs are included in the Supporting information. The most typical relaxation response (Figure 2C) demonstrates how the peaks are first shifted to slightly lower temperatures with the first t_a increases (the so-called upper peak behavior[31,32]), and only from $t_a \approx 300$ min the T_p starts to gradually increase with t_a—the sign of the so-called main peaks.[31,32] The atypical behavior depicted in Figure 2D shows a much less common case of the main and upper peaks being clearly separated, with the main peak emerging at the low-T shoulder and gradually increasing and overtaking the previously dominant upper peak.

The third set of graphs (Figure 2E,F) shows the evolution of T_p with $\delta_H{}^N$, where the superscript "N" denotes the normalized values of excess enthalpy evaluated from the $dT_f{\cdot}dT^{-1}$ signal instead of the real-life experimental heat flow or heat capacity signal. Note that the graphs were constructed by matching both quantities always evaluated for the identical t_a PS cycle. While the typical structural relaxation behavior manifests itself by the relatively pronounced increase of T_p (see Figure 2E), the low or negative $|\beta–x|$ difference leads to a large initial decrease of T_p in comparison with the consequent moderately scaled increase of the maximum temperature of the main relaxation peaks. What is most important are the values of the nonlinearity parameter evaluated from these data using the combination of Equations (6), (8), and (9). These values will be denoted as x_{out} (as "output") to differentiate them from the x values input into the simulations. The

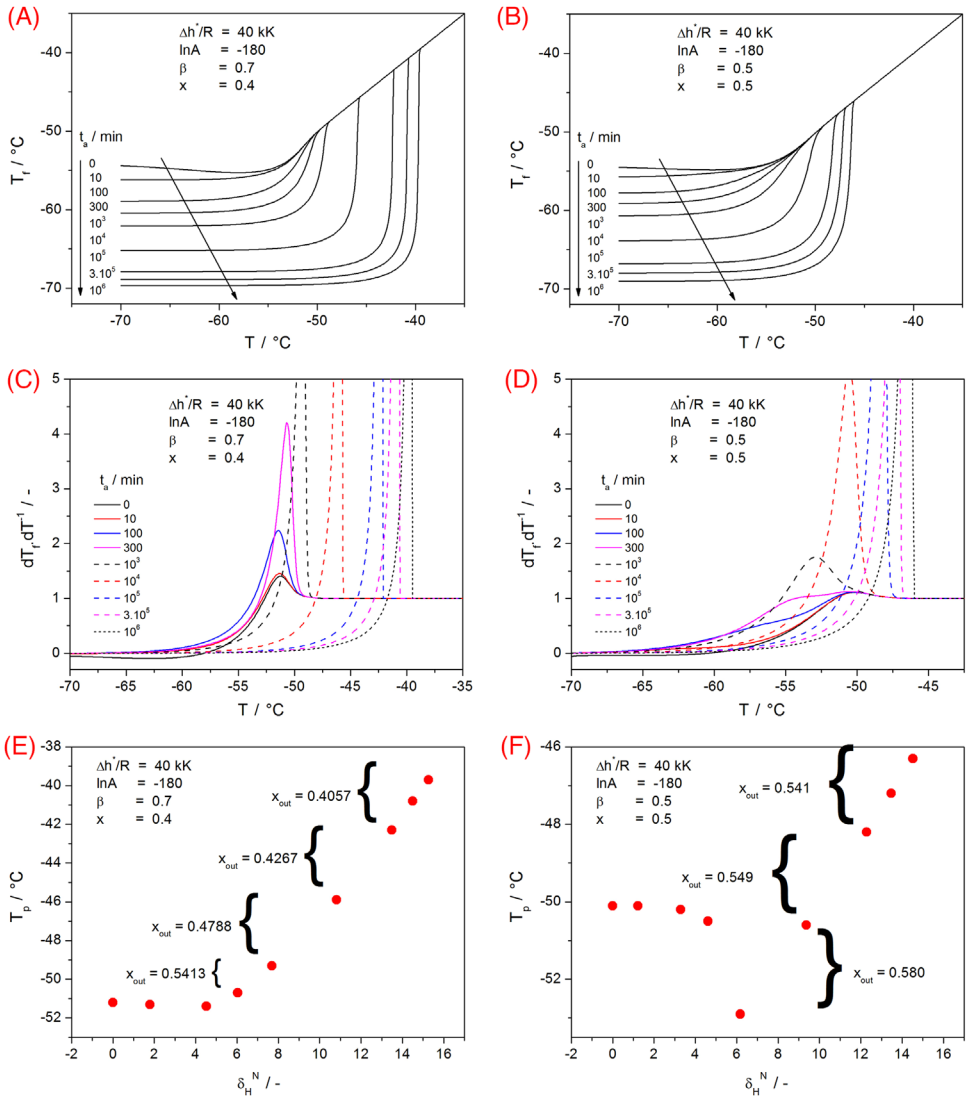

FIGURE 2 (A,B) Set of heating scans (displayed as T_f–T data) simulated as the parts of the PS method datasets for the mentioned combinations of the TNM parameters and the displayed series of t_as. (C,D) Set of heating scans (displayed as dT_f·dT^{-1}–T data) simulated as the parts of the PS method datasets for the mentioned combinations of the TNM parameters and the displayed series of t_as. (E,F) PS method T_p–$\delta_H{}^N$ dependencies evaluated for the data displayed in graphs C and D. The x_{out} values determined using Equations (6), (8), and (9) from the marked parts of the PS dependencies are indicated by the curly braces. PS, peak-shift; TNM, Tool–Narayanaswamy–Moynihan.

x_{out} values were in Figure 2E, F evaluated from the different segments of the simulated T_p–$\delta_H{}^N$ dependence, as is indicated in the graphs by the braces. It is evident that with increasing t_a, the slope of the dependences increases and the x_{out} evaluated from the later relaxation stages (segments of the dependence) decreases toward the correct value (the x value input into the simulations). For the common structural relaxation behavior (Figure 2E), the errors for the x_{out} determination are: ~ 1.5% in the 2 months to 2 years range, ~ 7% in the 1 week to 2 months range, ~ 20% in the 1 day to 1 week range, and ~ 35% in the 5 h to 1 day range. In other words, the acceptable level of precision is achieved only during extremely long t_as inconsistent with routine laboratory practice. Even more interesting is the result for the atypical glass behavior (Figure 2F), where the errors exhibit the span in the 8%–16% range, and the approach to the "correct" x value is very slow (cannot be practically reached even after a decade).

The influence of the relaxation rate (represented by the different β and x combinations) on the shape of the PS dependence is profiled across the tested β and x ranges in Figure 3. This is a characteristic profile, that is, practically universal for the absolute majority of glassy materials. In order to reveal the influence of the relaxation rate parameters on the shape of the PS dependence, we have calculated the correlation coefficients r between x, β, and (β–x) on one side, and maximum $\delta_H{}^N$, $t_a{}^{ons}$ (onset t_a, when the main peak first overrules the upper peak) and $\Delta T_p = T_p{}^{max} - T_p{}^0$

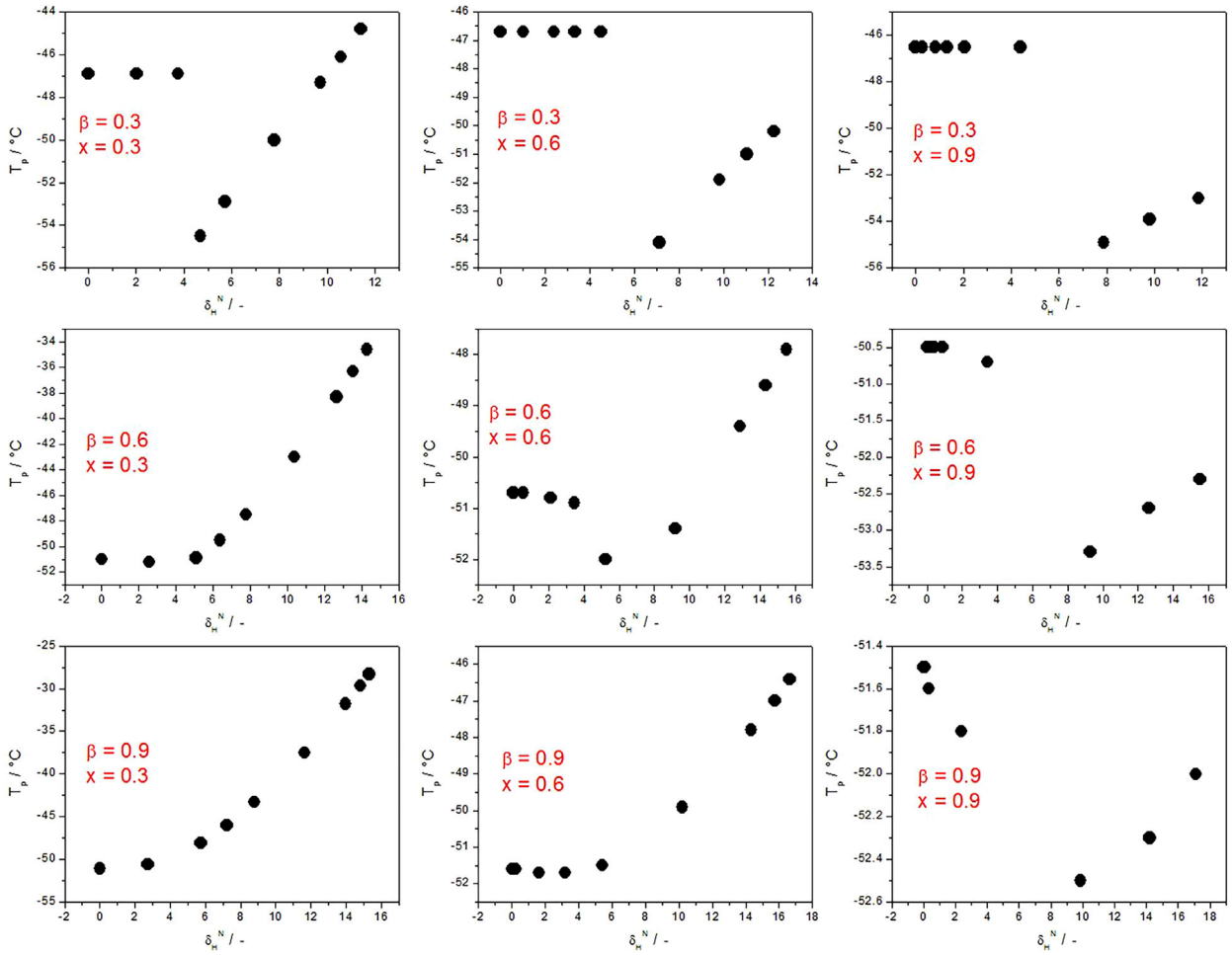

FIGURE 3 Selected PS dependencies simulated for $\Delta h^*/R = 40$ kK, $\ln(A/s) = -180$, $T_a = -70$°C, and displayed β and x combinations. PS, peak-shift.

(where the superscript denotes t_a) on the other side. The evaluations were done over the whole tested ranges of β and x, that is, 0.3–0.9 for both quantities (49 combinations in total). The following three correlations were found to be relevant: (β–x) versus ΔT_p with $r = 0.907$, x versus $t_a{}^{\text{ons}}$ with $r = 0.953$, and β versus maximum $\delta_{\text{H}}{}^{\text{N}}$ with $r = 0.911$. From the practical point of view, it is the first two correlations that are most relevant. The ΔT_p determines the evaluation precision—note that the reliability of the real-life T_p determination is worse than ± 0.1°C and even the present simulations performed at the 0.1°C precision level were affected by the "low" temperature resolution in certain cases, as will be discussed later. Hence, the higher ΔT_p decreases the requirements for precise evaluation of T_p. The $t_a{}^{\text{ons}}$ then determines the time-demanding nature of the experiments; note however that $t_a{}^{\text{ons}}$ is still not the t_a suitable for the determination of x_{out}, it is only the time from which the recorded data should start to be monitored.

In order to further test various aspects of the relaxation behavior, several other datasets (alternative to the one so far commented, i.e., $\Delta h^*/R = 40$ kK, $\ln(A/s) = -180$ and $T_a = -70$°C) were prepared. The influence of T_a was tested by simulating and evaluating two other datasets with $T_a = -60$ and -80°C. The profiled PS dependences (figures analogous to Figure 3) are included in the Supporting information. In the case of $T_a = -60$°C, the relaxation was in certain cases quite quick, and the equilibrium was reached before the main peak could have properly started to relax and exhibit the proper T_p shifts—at low β values, the shape (and therefore the evaluation) was still largely unaffected, but at higher β the evaluation of the PS dependences was very subjective due to the distortions caused by reaching the structural equilibrium. On the other hand, in the case of $T_a = -80$°C, the relaxation was extremely slow for simulations employing high x values (≥ 0.7), and the main peaks were not occurring even at the longest t_as. These tests indicate that there is always a T_a sweet-spot that should be attempted to obtain a suitable distortion-free PS dependence.

In addition to the influence of T_a, the effect of changing Δh^* was also explored—two additional datasets were simulated: (1) for $\Delta h^*/R = 80$ kK, $\ln(A/s) = -360$ and

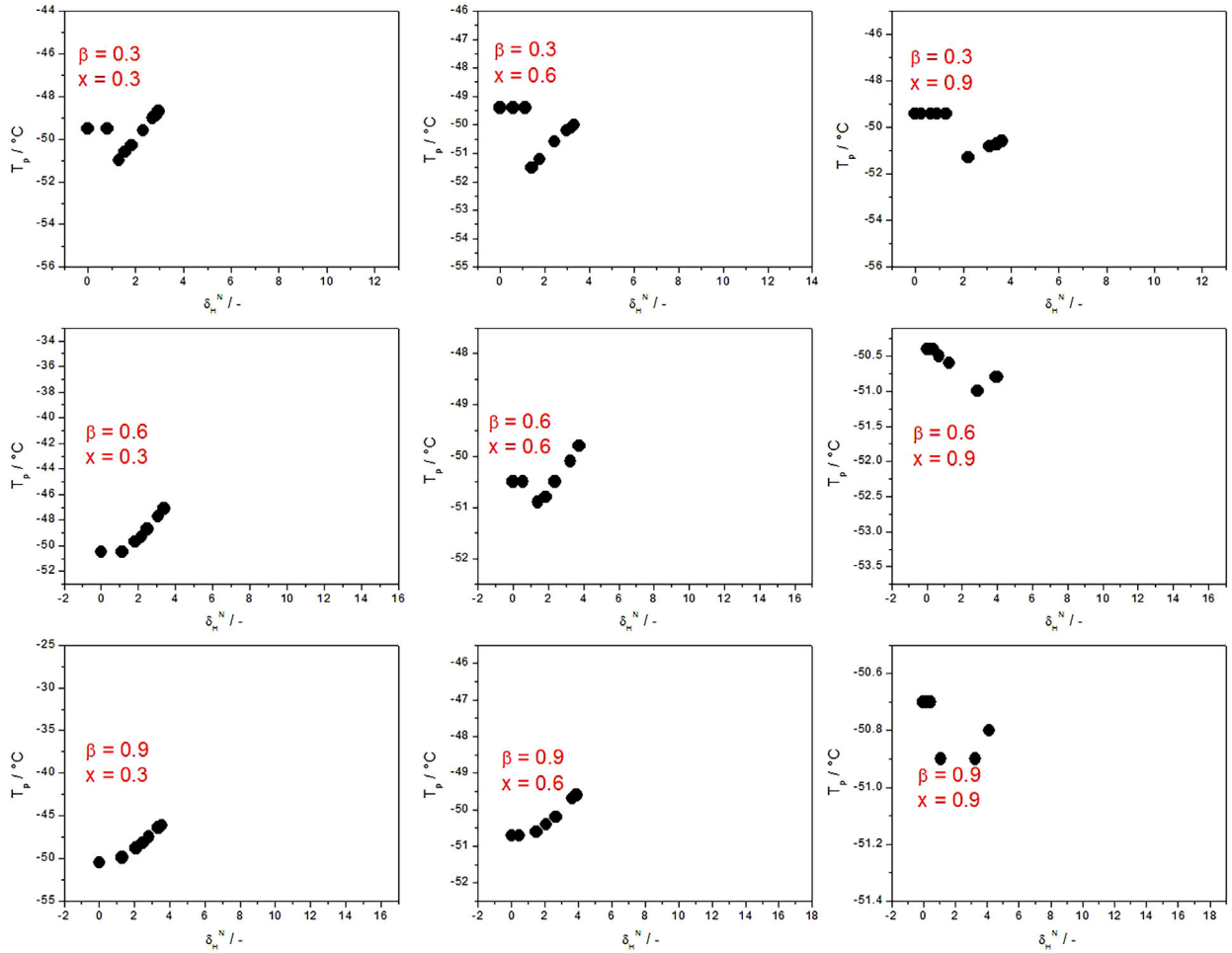

FIGURE 4 Selected PS dependencies simulated for $\Delta h^*/R = 160$ kK, $\ln(A/s) = -720$ and $T_a = -55°C$, and displayed β and x combinations. PS, peak-shift.

$T_a = -60°C$; (2) for $\Delta h^*/R = 160$ kK, $\ln(A/s) = -720$ and $T_a = -55°C$. This range of tested $\Delta h^*/R$ values covers an absolute majority of apparent activation energies reported for the glassy materials.[2] Note that the $\ln A$ values were adjusted accordingly to preserve the $T_g \approx -55°C$, and the above-mentioned $T_a s$ already represent the sweet-spot values, where the evaluation is least distorted. The profiled PS dependence for the dataset with $\Delta h^*/R = 80$ kK is included in the Supporting information; the selected results for the dataset with $\Delta h^*/R = 160$ kK are shown in Figure 4. As is immediately apparent, the shape of the dependences remains practically unchanged with respect to the corresponding β and x combinations, only the "dimensions" along both axes are shrunk. This is an expected result as the increased activation energy makes the relaxation process much less sensitive to the changes of the experimental conditions, such as, for example, the increase of t_a (after reaching the point at which the energetic barriers can be overcome). This indicates that the PS method is also largely independent of the influence of the apparent activation energy.

The summarized quantification of the PS method simulations performed within the framework of the first data batch (with $T_g \approx -55°C$) is shown in Figure 5—the quantity Δx_{out} defined as:

$$\Delta x_{out} = x_{out} - x. \tag{12}$$

Note that these graphs summarize more than 2200 different combinations of Δh^*, $\ln A$, β, x, T_a, and t_a. The graphs show that the proper choice of T_a is crucial for a precise and artifacts-free evaluation of x_{out} by the PS method. Most importantly, Figure 5A,D,E demonstrates the universality of the PS method (and of its intrinsic errors) with respect to different values of apparent activation energy Δh^*. Regarding the trends associated with varying β and x combinations, under most circumstances, the PS method tends to slightly overestimate (by 0.05–0.10) the evaluated nonlinearity parameter x. However, for low β paired with high x, the Δx_{out} overturns and exhibits quite large errors of ~ -0.20.

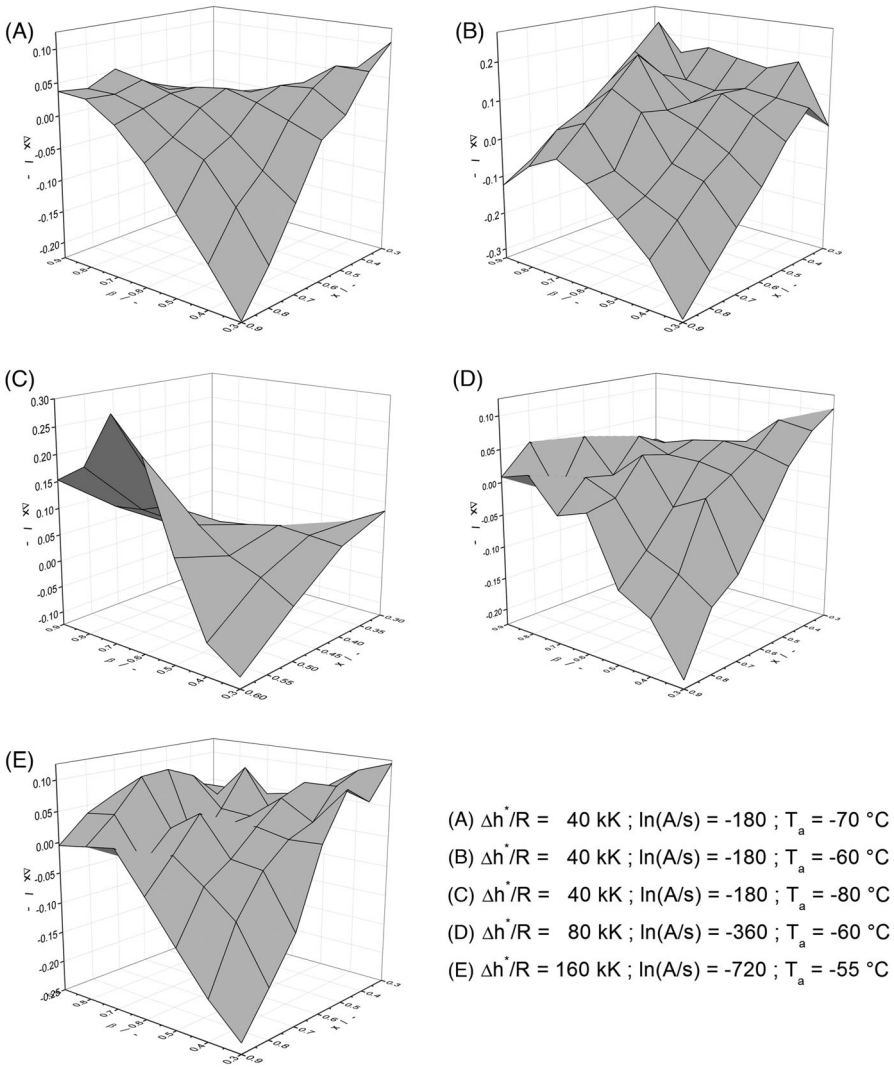

FIGURE 5 Magnitude of the errors/deviations of the nonlinearity parameter x_{out} as provided by the PS method applied in the cases of the theoretical datasets simulated for the given β and x combinations (indicated by X and Y axes) and other conditions listed in the in-graph legend. PS, peak-shift.

4 | DISCUSSION

This section will be split into the following sub-sections. In the first sub-section, the practical consequences of the results presented in the previous section will be discussed. In the second sub-section, further simulated data will be shown to demonstrate the universality of the present findings and conclusions. In the third sub-section, several experimental examples of the PS method utilization will be shown and commented on.

4.1 | Best practice for the peak-shift method

It was shown in Section 3 how the performance of the PS method changes for different materials and experimental (simulated) conditions. From the practical point of view, it is best to first asses the material with unknown structural relaxation behavior using the simple cooling→heating cycle (performed at $q^- > q^+$)—see Figure 6 for the profiled examples of the archetypal $dT_f \cdot dT^{-1}$–T curves simulated for $q^- = 50°C \cdot min^{-1}$ and $q^+ = 10°C \cdot min^{-1}$. Of particular interest is the presence of the "undershoot" (small exothermic dip preceding the glass transition onset), occurrence of the split main and upper peaks, and the height of the relaxation peak. In the second step, the suitable T_a temperature needs to be found. Depending on the activation energy and T_g of the investigated material, the suitable T_a may be between ~ (T_g–5°C) and (T_g–300°C). The data from Figure 6 corresponding to the samples relaxed at the sweet-spot T_a can serve as a guide for the correct choice of T_a—the curves were simulated for the t_a = 100 min. In accordance, the real-life sample can be screened at

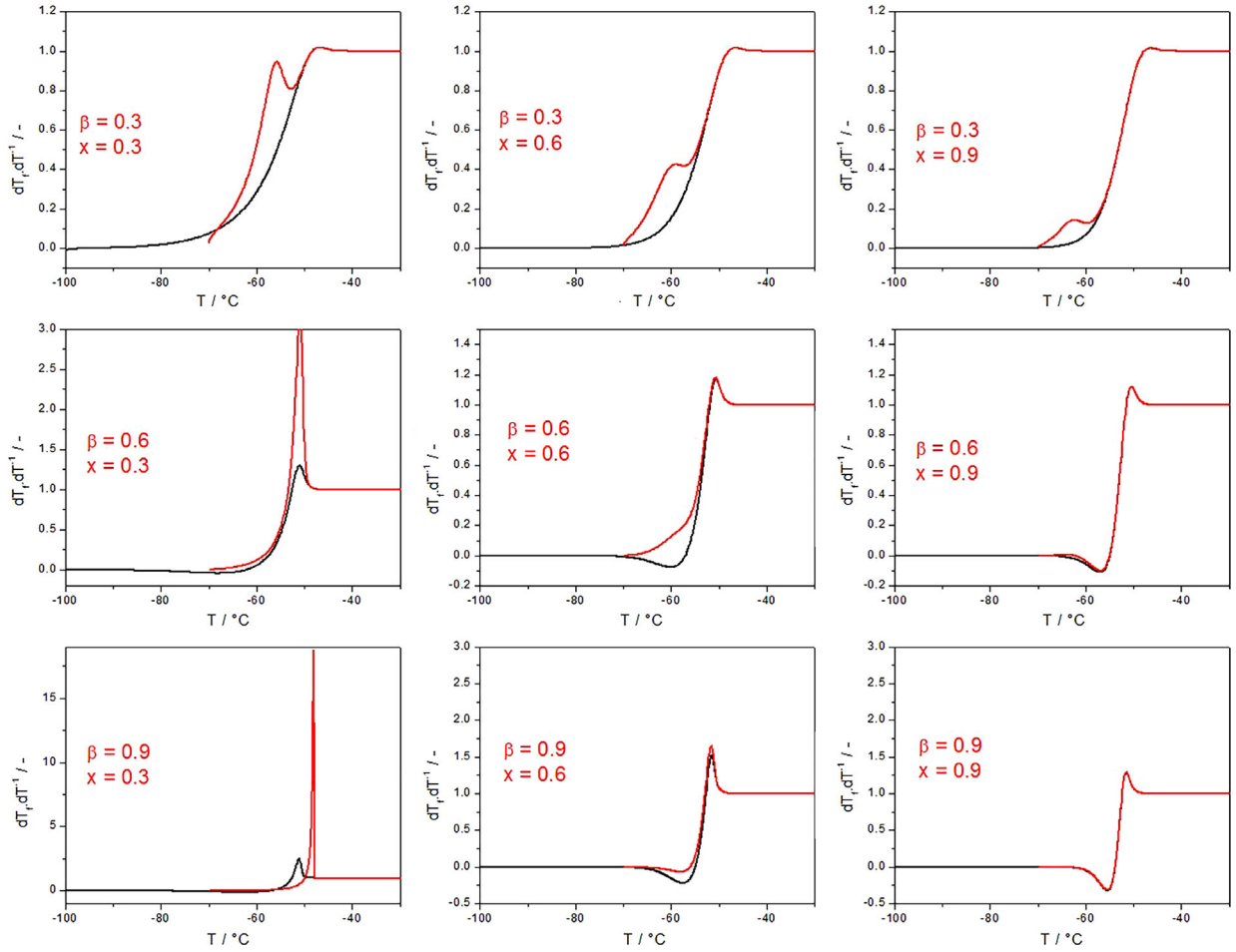

FIGURE 6 Archetypal $dT_f{\cdot}dT^{-1}$–T curves simulated for $q^- = 50°C{\cdot}min^{-1}$, $q^+ = 10°C{\cdot}min^{-1}$, $\Delta h^*/R = 40$ kK, $\ln(A/s) = -180$, and displayed β and x combinations. Black curves correspond to $t_a = 0$; red curves correspond to $t_a = 100$ min at $T_a = -70°C$.

different T_as, always applying $t_a = 100$ min, and the consequent pair of the heating measurements (at $t_a = 0$ and 100 min), the evolution of which is most reminiscent to the theoretical simulation depicted in Figure 6 is the one closest to the suitable T_a. Note that in the case of doubt, the T_as closer to T_g should always be checked/tested first. Owing to the universality of the general trends of the PS dependences, the data from Figure 3 can also be used as a rough prediction for the expected T_p and $\delta_H{}^N$ values at given t_as. The comparison of these predictions (dependences from Figure 3) with the first few experimentally obtained data points can be used to either adjust the estimated β and x combination or to skip certain t_a cycles to focus directly on the annealing times with suitable duration.

In practice, an issue can be associated with the correct determination of $\delta_H{}^N$ (the integration utilizing the course of the heat capacity in the glass region Δc_{pg}) for the non-relaxed glass ($t_a = 0$). For certain materials, the relaxation can be relatively quick at T_a, which distorts the baseline of the heating scan following the very short (or zero) annealing when the glassy structure does not have time to become compact enough for the immediate onset of the relaxation peak not to occur. This issue could be avoided if the sample could be cooled well below T_a after the relaxation step (characterized by T_a and t_a) without any additional consequences to the relaxation behavior of the material. In order words, the question is whether the relaxation at $T < T_a$ is negligible and whether the additional cooling step inserted in-between the annealing at T_a and the consequent heating scan would influence the results of the PS method. This hypothesis was tested in terms of three specifically designed temperature programs shown in Figure 7A,C. In Figure 7A, a standard PS method temperature program is shown, where the annealing at T_a is immediately followed by the heating scan from which T_p and $\delta_H{}^N$ are determined. The second program employs prolonged cooling (to lower T) during the $t_a = 0$ min cycle, and the third program further adds similar cooling segments at the end of all annealing steps. If T_f does not significantly change as a consequence of these added cooling segments, then the temperature program depicted in Figure 7C has the added benefit of the heating steps being performed from

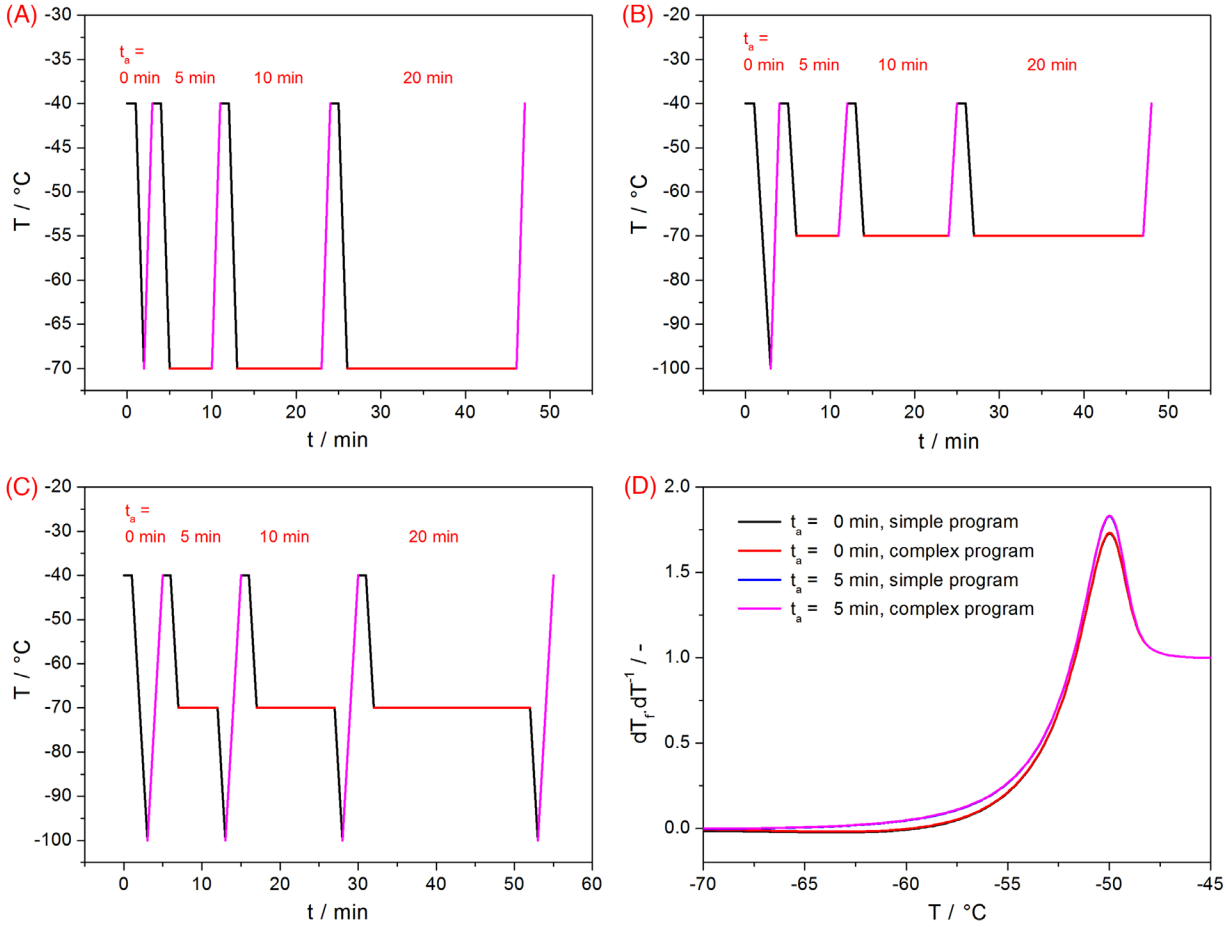

FIGURE 7 (A)–(C) Three different types of PS temperature programs differing in the presence of additional cooling steps following the annealing program segments. (D) Simulated heating scans corresponding to the PS temperature programs displayed in graph A ("simple" program) and graph C ("complex" program). The pairs of curves simulated for the same t_as overlap perfectly. PS, peak-shift.

low T and not having any features (undershoot, course of baseline, …) masked by the glass transition peak onsetting immediately at the start of the heating step. The programs were tested for the following combination of the relaxation parameters: $\Delta h^*/R = 40$ kK, $\ln(A/s) = -180$, $\beta = 0.7$, $x = 0.4$. Note that these parameters represent a material that shows a fast relaxation rate. The dT_f·dT^{-1}–T signals simulated for the heating scans performed after the annealing steps with $t_a = 0$ and 5 min (the two cases most prone to distortions) are shown in Figure 7D. The standard temperature program (Figure 7A) is denoted as "simple"; the program with included additional cooling segments to low T is denoted as "complex". As is apparent, the curves for the simple and complex programs perfectly overlap, which indicates that T_f achieved during the preceding annealing/cooling steps were identical. Also, as expected, all three temperature programs depicted in Figure 7A–C provided an exactly similar value of x_{out} evaluated by means of the PS method. This finding confirms the "complex" PS method to be a suitable solution for the materials that at optimum T_a do not show a steady constant course of the baseline in the derivative (dT_f·dT^{-1}) data. Note however, that the original "simple" PS method is still in practice preferred in the cases when the complex temperature program is not necessary because the simple temperature program is shorter (less chance for baseline drift) and the lack of additional cooling segments improves reproducibility of the c_p signal.

4.2 | Universality of the PS method

So far, the PS method was tested only for the relaxation processes occurring at a very low T of ≈ −55°C. In order to confirm the general nature of the derived conclusions, further batches of similar tests were also performed for other T_g values of ≈ 50, 200, 600, and 1000°C, which covers the temperature range, where the glass transition for the absolute majority of materials can be found. For each of these T_g values, two datasets corresponding to $\Delta h^*/R = 40$ and 160 kK were explored. The $\ln(A/s)$ values used to achieve the above-mentioned T_gs for these pre-selected activation

TABLE 1 Values of the reduced apparent activation energy $\Delta h^* \cdot R^{-1}$ and pre-exponential factor A input into the simulations for the simulated curves to exhibit the listed T_g.

T_g (°C)	$\Delta h^* \cdot R^{-1}$ (kK)	ln(A/s)
−55	40	−180
−55	160	−720
50	40	−123
50	160	−492
200	40	−83
200	160	−338
600	40	−43
600	160	−182
1000	40	−28
1000	160	−124

energies are listed in Table 1. In accordance with the simulations shown in Section 3, sets of PS cycles were simulated with β and x varying in the 0.3–0.9 ranges (with the 0.1 step) for each combination of Δh^* and ln$A$ shown in Table 1. In this way, additional 392 sets (3528 PS unique PS cycles) of different types of structural relaxation behavior were simulated and evaluated in terms of the PS method. The resulting summarized quantification of the errors (Δx_{out}) associated with the usage of the PS method for different types of structural relaxation behavior—as expressed by the different combinations of Δh^*, A, β, and x—is shown in Figure 8. The remarkable similarity (both, in the shape and absolute Δx_{out} values) of the hyper-surfaces introduced in Figure 8 unambiguously confirms the universality of the conclusions based on these data, and their validity for practically all glassy/amorphous materials. The following conclusions can be derived from these data:

1. in the majority of cases, the PS method slightly overestimates (by 0.05–0.10) the true value of the nonlinearity parameter.
2. the accuracy of x_{out} determination slightly decreases with the increase of T_g tested in the −50 to 1000°C temperature range).
3. the accuracy of x_{out} determination slightly decreases with Δh^* (tested for the reduced activation energies of 40 and 160 kK).
4. the accuracy of the PS method significantly decreases for the materials with high x and low β.

4.3 | Practical examples of the peak-shift method utilization

In this section, several examples of our older experimental data[42–46] (together with some unpublished results) will be presented to discuss certain practical aspects of this method. These PS dependencies are shown in Figure 9, together with the x values determined by the PS method and by the curve-fitting approach. Starting with Figure 9A and glassy selenium, the two data series demonstrate the difference between the aging at 27 and 29°C. The PS cycles performed at T_a = 29°C finished prematurely, reaching the structural equilibrium (represented by the undercooled liquid state), and the corresponding slope of the T_p–$\delta_H{}^N$ dependence led to x_{out} = 0.60 (which is still acceptable information with regard to at least qualitative classification of the material's relaxation behavior). The PS dependences for the selenium glasses doped with Te, As, and Ge are shown in Figure 9B–D. Here, the PS dependencies are nicely linear at higher annealing times, which give higher confidence to their evaluation according to Equations (6), (8), and (9). Similar to the pure Se, the x_{out} values determined for these glasses by the PS method are remarkably similar to those obtained from the curve-fitting method. Considering the corresponding values of the non-exponentiality parameter β, which are 0.65, 0.83, 0.63, and 0.62 for the pure a-Se and Te-, As- and Ge-doped selenium glasses, respectively, the course of the PS dependencies depicted in Figure 9A–D very well agrees with their expected shape (as determined from the theoretically simulated data from Figure 3). It is noteworthy that the presence and magnitude of the "dip" (represented by the decrease of T_p at medium t_as) can be very well used as a rough estimate of the β/x ratio. A larger magnitude of the characteristic dip in the PS dependence can be observed in the case of the PVAc material—Figure 9E, where β determined from curve-fitting was 0.50. This is again in good agreement with the prediction based on the data from Figure 3. Very different shape of the PS dependence was recorded for the $Ge_2Sb_2Se_5$ glass (that, by the way, has also much higher T_g, confirming the universality of the present approach). For this material, the curve-fitting provided $\beta = 0.68 \pm 0.08$, which is practically similar to the x-value from the PS method (0.67 ± 0.03). The much larger magnitude of the dip and the final T_p values (obtained at largest applied t_a) still exceeding the initial T_p obtained at t_a = 0 min indicate (based on the comparison with Figure 3) that indeed $\beta/x \approx 1$ and the nonlinearity should be between 0.6 and 0.7.

5 | CONCLUSIONS

The performance of the PS method was tested by means of theoretical simulations. The method was found to provide fairly accurate of the nonlinearity parameter x, deviating in most cases by a maximum of 0.05–0.10. For the majority

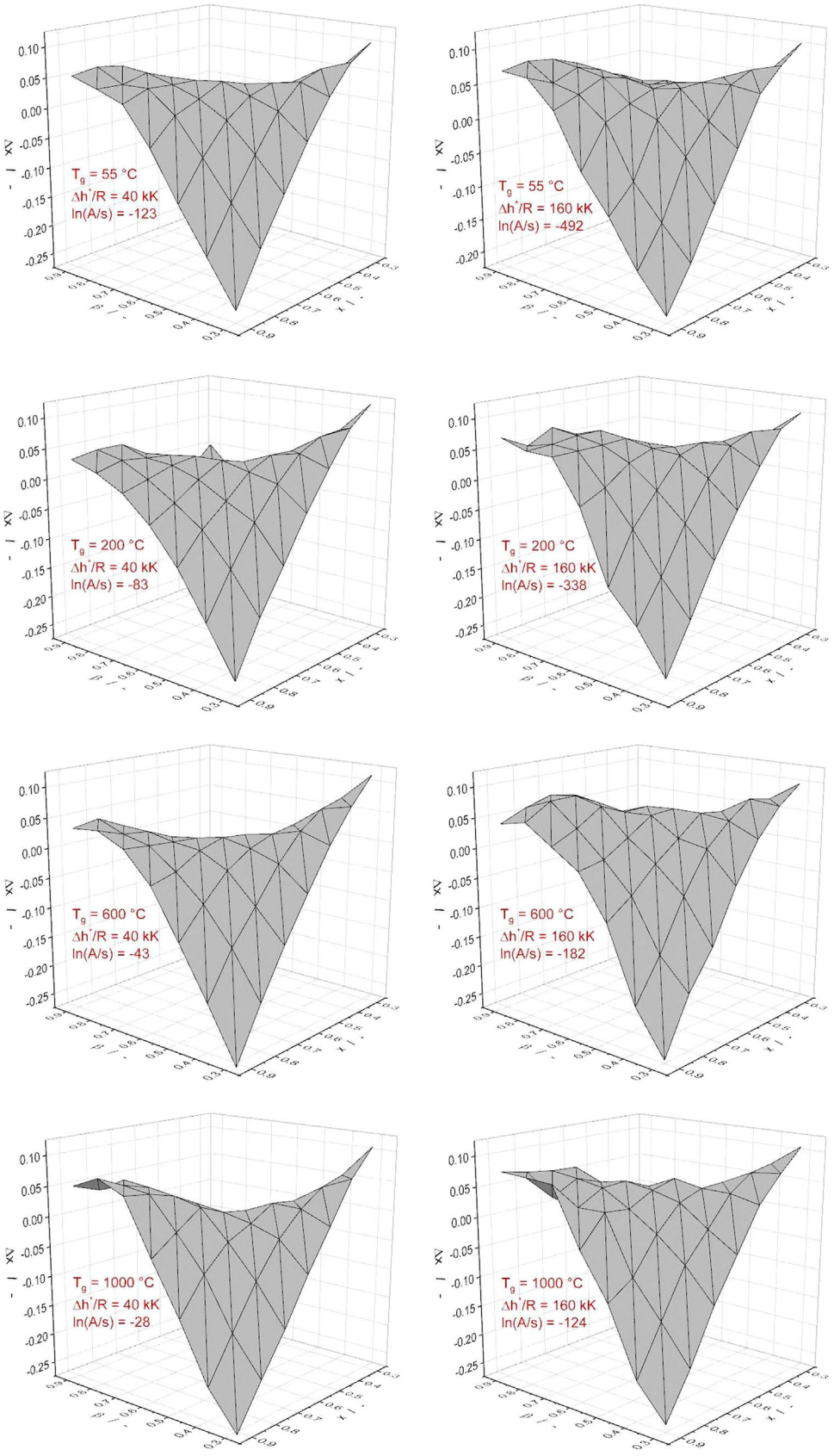

FIGURE 8 Magnitude of the errors/deviations of the nonlinearity parameter x_{out} as provided by the PS method applied in the cases of the theoretical datasets simulated for the given β and x combinations (indicated by X and Y axes). The approximate T_g values are listed in each graph together with the supplemental conditions for the simulations. PS, peak-shift.

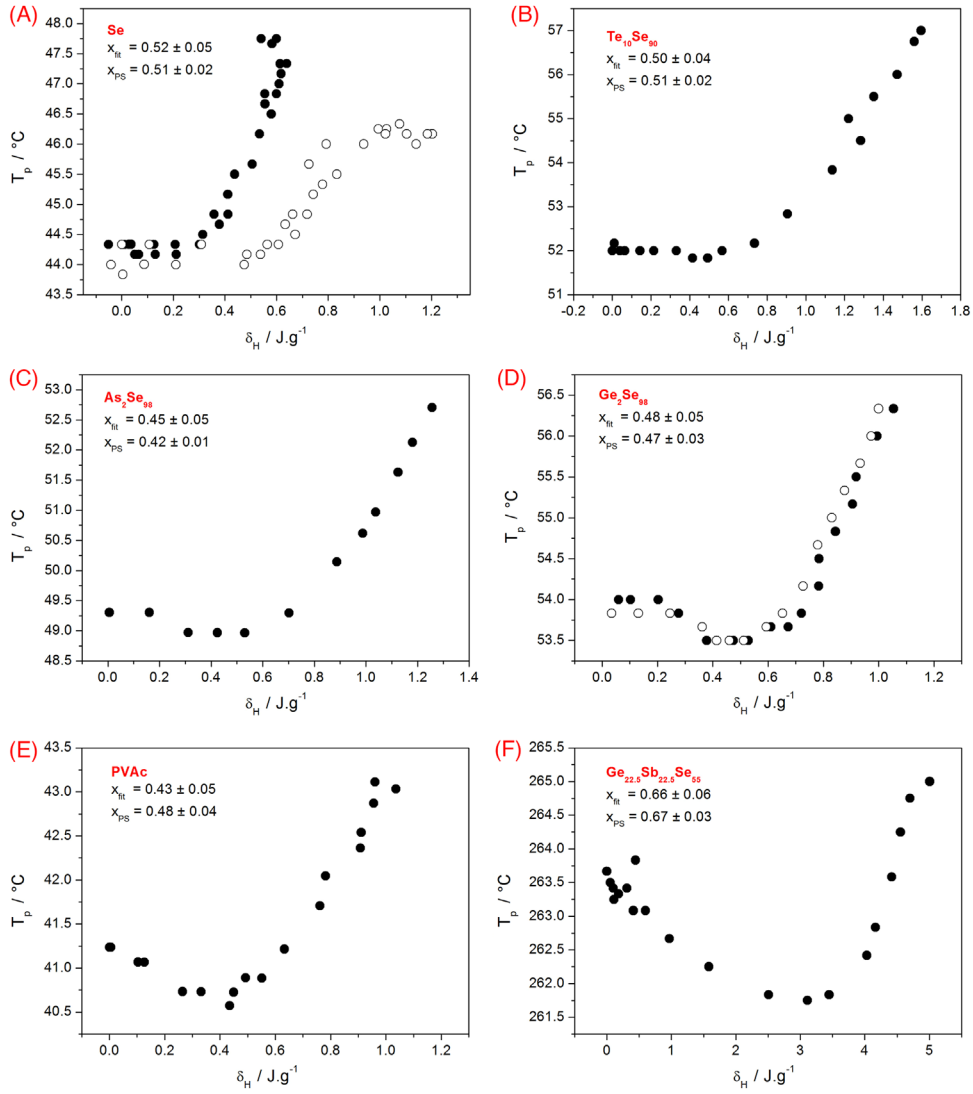

FIGURE 9 Experimental PS dependences for amorphous Se (full points correspond to $T_a = 27°C$, empty points correspond to $T_a = 29°C$),[42] $Te_{10}Se_{90}$,[45] As_2Se_{98},[44] Ge_2Se_{98},[44] PVAc,[43] and $Ge_{22.5}Sb_{22.5}Se_{55}$[46]. PS, peak-shift.

of types of structural relaxation behavior (characterized by the different combinations of the TNM parameters β and x), the PS method tends to slightly overestimate the value of x. In the specific cases when $\beta/x \leq 0.3$, the PS method systematically largely underestimates the nonlinearity parameter—this type of structural relaxation behavior is however very rare. The universality of the PS method performance was verified for practically all glassy/amorphous materials, for which the $dT_f \cdot dT^{-1}$ data are usually collected: glass transition temperature T_g values between −55 and 1000°C, the reduced activation energy of structural relaxation $\Delta h^*/R$ between 40 and 160 kK. The importance of the proper selection of the annealing temperature T_a was demonstrated. A new complex/improved temperature program for the PS method was proposed and theoretically tested—utilization of this temperature program eliminates the inaccuracies associated with the fast relaxation onset that can occur for certain materials. In addition, based on the comparison between the theoretically simulated and real-life experimental data, the usefulness of the characteristic PS dependence shape for the rough complementary estimate of the non-exponentiality β parameter was introduced.

ACKNOWLEDGMENTS

This work was supported by The Ministry of Education, Youth and Sports of the Czech Republic (LM2023037).

ORCID

Roman Svoboda https://orcid.org/0000-0002-1253-366X

REFERENCES

1. Scherer GW. Relaxation in glass and composites. New York; Wiley; 1986.

2. Hodge IM. Enthalpy relaxation and recovery in amorphous materials. J Non-Cryst Sol. 1994;169:211–66.
3. Kovacs AJ, Aklonis JJ, Hutchinson JM, Ramos AR. Isobaric volume and enthalpy recovery of glasses. II. A transparent multiparameter theory. J Polym Sci. 1979;17:1097–162.
4. Hutchinson JM, Ruddy M, Wilson MR. Differential scanning calorimetry of polymer glasses: corrections for thermal lag. Polymer. 1988;29:152–9.
5. McCrum NG, Buckley CP, Bucknall CB. Principles of polymer engineering. New York: Oxford University Press; 1997.
6. Robertson RE, Simha R, Curro JG. Free volume and the kinetics of aging of polymer glasses. Macromolecules. 1984;17:911–9.
7. Ngai KL. Universality of low-frequency fluctuation, dissipation and relaxation properties of condensed matter. I. Comment Solid State Phys. 1979, 9:127–40.
8. Ngai KL. Universality of low-frequency fluctuation, dissipation and relaxation properties of condensed matter. II. Comment Solid State Phys. 1980;9:141–55.
9. Ngai KL, Rendell RW, Rajagopal AK, Teitler S. Three coupled relations for relaxations in complex systems. Ann NY Acad Sci. 1986;484:150–84.
10. Hodge IM. Adam–Gibbs formulation of nonlinearity in glassy-state relaxations. Macromolecules. 1986;19:936-8.
11. Debenedetti PG, Stillinger FH. Supercooled liquids and the glass transition. Nature. 2001;410:259–67.
12. Struik LCE. Physical aging of amorphous polymers and other materials. New York: Elsevier; 1978.
13. Struik LCE. On volume-recovery theory: 2. test on Kovacs's original δ vs. t data. Polymer. 1997;38:5233–41.
14. McKenna GB, Vangel MG, Rukhin AL, Leigh SD, Lotz B, Straupe C. The τ-effective paradox revisited: an extended analysis of Kovacs' volume recovery data on poly(vinyl acetate). Polymer. 1999;40:5183–205.
15. Donth E, Hempel E. Structural relaxation above the glass temperature: pulse response simulation with the Narayanaswamy Moynihan model for glass transition. J Non-Cryst Solids. 2002;306:76-89.
16. Aharoune A, Marceron-Balland P, Cunat C. The DNLR approach and relaxation phenomena. Part II—application: volume recovery of PVAc. Comparison between the DNLR approach and some other modellings. Mech Time Depend Mater. 2001;5(4):345–77.
17. Delin M, Rychwalski RW, Kubát J, Klason C, Hutchinson JM. Physical aging time scales and rates for poly(vinyl acetate) stimulated mechanically in the T_g-region. Polym Eng Sci. 1996;36:2955–67.
18. Cowie JMG, Harris S, McEwen IJ. Physical aging in poly(vinyl acetate). 2. Relative rates of volume and enthalpy relaxation. Macromolecules. 1998;31(8):2611–5.
19. McKinney JE, Goldstein M. PVT relationships for liquid and glassy poly(vinyl acetate). J Res Nat Bur Stand. 1974;A78:331–53.
20. Hutchinson JM, Kumar P. Enthalpy relaxation in polyvinyl acetate. Thermochim Acta. 2002;391(1–2):197–217.
21. Sasabe H, Moynihan CT. Structural relaxation in polyvinyl acetate. J Polym Sci. 1978;16:1447–57.
22. Tool AQ. Relation between inelastic deformability and thermal expansion of glass in its annealing range. J Am Ceram Soc. 1946;29:240–53.
23. Narayanaswamy OS. A model of structural relaxation in glass. J Am Ceram Soc. 1971, 54:491–7.
24. Moynihan CT, Easteal AJ, DeBolt MA, Tucker J. Dependence of the fictive temperature of glass on cooling rate. J Am Ceram Soc. 1976;59:12–6.
25. Hodge IM, Berens AR. Effects of annealing and prior history on enthalpy relaxation in glassy polymers. 2. Mathematical modeling. Macromolecules. 1982;15:762–70.
26. Svoboda R. Utilization of "q^+/q^- = const." DSC cycles for enthalpy relaxation studies. Eur Polym J. 2014;59:180–8
27. Svoboda R. Novel equation to determine activation energy of enthalpy relaxation. J Therm Anal Calorim. 2015;121:895–9.
28. Svoboda R. Utilization of constant heating rate DSC cycles for enthalpy relaxation studies and their influenceability by error data-distortive operations. J Non-Cryst Sol. 2015;408:115–22.
29. Svoboda R, Málek J. Enthalpy relaxation in Ge–Se glassy system. J Therm Anal Cal. 2013;113:831–42
30. Svoboda R, Málek J. Description of macroscopic relaxation dynamics in glasses. J Non-Cryst Solids. 2013;378:186–95.
31. Hutchinson JM, Kovacs AJ. Effects of thermal history on structural recovery of glasses during isobaric heating. Polym Eng Sci. 1984;24:1087–103.
32. Hutchinson JM, Ruddy M. Thermal cycling of glasses. II. Experimental evaluation of the structure (or nonlinearity) parameter x. J Polym Sci. 1988;B26:2341–66.
33. Ramos AR, Hutchinson JM, Kovacs AJ. Isobaric thermal behavior of glasses during uniform cooling and heating. III. Predictions from the multiparameter KAHR model. J Polym Sci B. 1984;22(9):1655–96
34. Slobodian P, Zatloukal M, Sáha P. Evaluation of the structure (or nonlinearity) parameter x by peak-shift method from volumetric heating data of PET. J Phys Chem Sol. 2008;69:975–80.
35. Montserrat S, Cortés P, Pappin AJ, Quah KH, Hutchinson JM. Structural relaxation in fully cured epoxy resins. J Non-Cryst Solids. 1994;172–174:1017–22.
36. Clarkson C. Enthalpy relaxation of a DGEBA epoxy as a function of time, temperature, and cooling rate. Bulletin of the American Physical Society. AMS; 2015.
37. Abu-Sehly AA, Elabbar AA. Physical aging in Bi5Se95 chalcogenide glass: effect of annealing time and temperature. Dig J Nanomater Biostructures. 2012;7:763–70.
38. Ramírez, C., Abad, M.J., Cano, J, López J, Nogueira P, Barral L. Enthalpy relaxation in an epoxy-cycloaliphatic amine resin. Colloid Polym Sci. 2001;279:184–9.
39. Poorabdollah M, Beheshty MH, Atai M. Investigating curing kinetics and structural relaxation phenomena of unsaturated polyester resin containing silanized silica. J Compos Mater. 2016;50:2459–67
40. Deepika, Rathore K, Saxena NS. Kinetics of phase transformations and thermal stability of $Se_{58}Ge_{42-x}Pb_x$ ($x = 15$, 18, and 20) glasses. New J Glass Ceram. 2012;2:23–33.
41. https://omnexus.specialchem.com/polymer-properties/properties/glass-transition-temperature
42. Svoboda R, Pustková P, Málek J. Relaxation behavior of glassy selenium. J Phys Chem Sol. 2007;68:850–4.
43. Svoboda R, Pustková P, Málek J. Structural relaxation of polyvinyl acetate (PVAc). Polymer. 2008;49:3176–85
44. Svoboda R, Pustková P, Málek J. Relaxation in Ge_2Se_{98} and As_2Se_{98} glasses. J Non-Cryst Solids. 2010;356:447–55.

45. Svoboda R, Honcová P, Málek J. Enthalpic structural relaxation in Te–Se glassy system. J Non-Cryst Solids. 2011;357:2163–9.
46. Svoboda R, Honcová P, Málek J. Enthalpic relaxation in $Ge_2Sb_2Se_5$ glass. J Non-Cryst Solids. 2012;358:804–9

SUPPORTING INFORMATION

Additional supporting information can be found online in the Supporting Information section at the end of this article.

How to cite this article: Svoboda R. The peak-shift method for the description of structural relaxation in glassy materials: a critical review. J Am Ceram Soc. 2023;106:5233–5247. https://doi.org/10.1111/jace.19172